Modern Aspects of Electrochemistry 54

Stojan S. Djokić *Editor*

Electrochemical Production of Metal Powders

Springer

MODERN ASPECTS OF ELECTROCHEMISTRY

No. 54

For further volumes:
http://www.springer.com/series/6251

Previously from Modern Aspects of Electrochemistry

Modern Aspects of Electrochemistry No. 52

Applications of Electrochemistry and Nanotechnology in Biology and Medicine I

Edited by Noam Eliaz, Professor of Engineering at Tel-Aviv University

Topics in Number 52 include:

- Monitoring of cellular dynamics with electrochemical detection techniques
- Fundamental studies of long- and short-range electron exchange mechanisms between electrodes and proteins
- Microbial fuel cell scalability and applications in robotics
- Electrochemical coating of medical implants
- Electrochemical techniques for obtaining biofunctional materials
- Preparation and properties of bioactive metals prepared by surface modification

Modern Aspects of Electrochemistry No. 53

Applications of Electrochemistry and Nanotechnology in Biology and Medicine II

Edited by Noam Eliaz, Professor of Engineering at Tel-Aviv University

Topics in Number 53 include:

- Fundamental studies of electron tunneling between electrodes and proteins
- Electron transfer kinetics at oxide films on metallic biomaterials
- How adsorption of organic molecules and ions depends on surface crystallography of the metal electrode
- Studying and modifying biomaterial surfaces with high resolution using the scanning electrochemical microscope
- Electrochemical method for high-throughput screening of enzymatic activity

Stojan S. Djokić
Editor

Electrochemical Production of Metal Powders

Springer

Editor
Stojan S. Djokić
Elchem Consulting Ltd.
Edmonton, AB, Canada

ISSN 0076-9924
ISBN 978-1-4614-2379-9 ISBN 978-1-4614-2380-5 (eBook)
DOI 10.1007/978-1-4614-2380-5
Springer New York Heidelberg Dordrecht London

Library of Congress Control Number: 2012934056

Printed on acid-free paper

Springer is part of Springer Science+Business Media (www.springer.com)

Preface

The present volume of *Modern Aspects of Electrochemistry* brings readers the newest developments and achievements in the production of metallic powders by electrochemical and electroless methods from aqueous solutions. Although the deposition of metallic powders from aqueous solutions was intensively studied for years, the last summarized results (Calusaru) on this topic were published in 1979.

Electrochemically and chemically produced metal powders from aqueous solutions are of high purity. These powders find applications in metallurgy, automotive, aerospace, energy device, electronics, and biomedical industries. Disperse deposits and electrochemically produced metal powders are also very suitable for use as catalytic surfaces in chemical industry.

This volume of *Modern Aspects of Electrochemistry* reviews the electrochemical aspects of the latest developments in the deposition of metal powders. Distinguished international contributors have written chapters devoted to this fine area which may impact significant technological advancement in the future. Following is a brief description of chapters in this volume of *Modern Aspects of Electrochemistry*.

Popov and Nikolić in Chapter 1 discuss the fundamental aspects of disperse metals electrodeposition. The shapes of polarization curves in relation to the deposition process parameters are analyzed. Disperse metal deposits are formed with a nonuniform current density

distribution over the surface of the macroelectrode. Adherent granular disperse deposits are produced in an electrodeposition process characterized by a large exchange current density, due to the formation of nucleation exclusion zones around growing grains on the inert substrate. Nonadherent dendritic or spongy deposits are formed in the dominant diffusion control on the level of the macroelectrode and an activation control on the tips of microelectrodes placed inside the diffusion layer of the macroelectrode. Nonadherent honeycomb-like deposit is formed in the presence of strong hydrogen codeposition. All the above cases are discussed in detail and explained using appropriate mathematical models. It is also shown that the formation of dendritic deposits at low level of coarseness strongly increases the apparent exchange current density for the deposition process, producing electrocatalytic effect.

Chapter 2, by Jović et al., presents the results of morphology investigation of different metal powders, e.g., Ag, Pd, Pb, Cd, Fe, Ni, and Co. It is shown that the morphology is different for each metal. The conditions for deposition of each powder are specified. Diffusion control, based on the descriptions in this chapter, is necessary for the formation of powders in accordance with the current theory. Presented results correspond to either disperse deposits on the electrode or powders spontaneously detached or removed by tapping from the electrode.

In Chapter 3, by Nikolić and Popov, types, properties, and modeling of copper powders are presented. Powdered copper deposits are formed at overpotentials and current densities belonging to the plateau of the limiting diffusion current density and/or at higher, where the simultaneous hydrogen evolution reaction occurs. The effect of periodically changing regimes of electrolysis, such as pulsating current, reversing current, and pulsating overpotential, on the formation of disperse copper deposits is analyzed. It is shown that the effects on morphology of electrodeposited copper with an application of square-waves pulsating current are equivalent to those attained by electrodepositions in the constant regimes of electrolysis from solutions of different $CuSO_4$ and H_2SO_4 concentrations.

Chapter 4, by Nikolić, discusses the formation of open and porous electrodes by the constant and periodically changing regimes of electrolysis. The formation of these electrodes in both potentiostatic

and galvanostatic electrodeposition is presented. Three dimensional foam or honeycomb-like copper electrodes are formed by electrochemical deposition at high current densities and overpotentials where parallel to copper electrodeposition, hydrogen evolution occurs. Hydrogen evolution enabling the formation of these electrodes is vigorous enough to cause such stirring of the copper solution which leads to the decrease of the cathode diffusion layer thickness and to the increase in the limiting diffusion current density and hence to the change of the hydrodynamic conditions in the near-electrode layer. The phenomenology of the formation of the honeycomb-like structures by potentiostatic electrodeposition, as well as parameters affecting number, size, and distribution holes in the honeycomb-like structures, is analyzed.

Jović et al. in Chapter 5 discuss morphology, chemical and phase composition of electrodeposited Co–Ni, Fe–Ni, and Mo–Ni–O powders. The processes of Co–Ni, Fe–Ni, and Mo–Ni–O powders electrodeposition were investigated by polarization measurements compensated for IR drop. All polarization curves were characterized with two inflection points. The first one, positioned at a less negative potential reflecting the onset of electrodeposition, is seen as a sudden increase in the current density and the second one, at more negative potential, is characterized by a decrease of the slope on the polarization curves, representing the stage when the electrodeposition becomes controlled by the rate of hydrogen bubbles formation. Powder samples for the investigation of morphology, chemical, and phase composition are electrodeposited at current density slightly lower than that corresponding to the second inflection point.

Chapter 6, by Magagnin and Cojocaru, is a review of recent progress in the electrochemical synthesis of dispersed nanoparticles, including the sonoelectrochemical approach. Results on the synthesis of silver and gold particles with size from the nanoscale to the mesoscale in sulfite-based solutions are reported. The electrochemical behavior of the electrolytes used in the electrodeposition is studied on different substrates such as glassy carbon, Ti, and indium tin oxide. Silver particles below 50 nm were easily obtained on glassy carbon substrate by potential-controlled deposition achieving a high nucleation density. Silver particle deposition on titanium showed low nucleation density and a strong tendency to form large particles,

clusters, and agglomerates, mostly in connection with surface irregularities. Gold particles were successfully deposited by either a potential pulse or a potential sweeping technique, achieving good results in terms of nucleation density. This was observed on titanium substrate, using a single potential pulse technique for the deposition of Au particles. The preparation of dispersed nanoparticles supported on silicon by galvanic displacement reactions in microemulsions is also presented. Examples of gold and palladium particles are included, discussing the mechanism of formation and the coalescence behavior of the nanostructures.

Finally, in Chapter 7 Djokić discusses the deposition of metallic powders from aqueous solutions without an external current source. Metallic powders can be successfully produced via galvanic displacement reaction or by electroless deposition from homogenous aqueous solutions or slurries. The formation of various metallic powders without an external current source e.g., Cu, Ni, Co, Ag, Pd, and Au, using appropriate reducing agents is presented. The mechanistic aspects of electroless deposition of powders are also discussed. It is shown that the hydrolysis of metallic ions is the most important factor leading to the deposition of metal powders from aqueous solutions.

This new volume of *Modern Aspects of Electrochemistry* brings to scientists, engineers, and students new concepts and summarized results in the fields of electrochemical and chemical deposition, which may have significant influence for future practical applications.

Edmonton, AB, Canada Stojan S. Djokić

Contents

Contributors

Paula Cojocaru Dip. Chimica, Materiali e Ing., Chimica G. Natta, Politecnico di Milano, Milano, Italy

Stojan S. Djokić Elchem Consulting Ltd., Edmonton, AB, Canada

Borka M. Jović Department of Materials Science, Institute for Multidisciplinary Research, University of Belgrade, Belgrade, Serbia

Vladimir D. Jović Department of Materials Science, Institute for Multidisciplinary Research, University of Belgrade, Belgrade, Serbia

Uroš Č. Lačnjevac Department of Materials Science, Institute for Multidisciplinary Research, University of Belgrade, Belgrade, Serbia

Luca Magagnin Dip. Chimica, Materiali e Ing., Chimica G. Natta, Politecnico di Milano, Milano, Italy

Nebojša D. Nikolić ICTM-Institute of Electrochemistry, University of Belgrade, Belgrade, Serbia

Konstantin I. Popov ICTM-Institute of Electrochemistry, University of Belgrade, Belgrade, Serbia

Faculty of Technology and Metallurgy, University of Belgrade, Belgrade, Serbia

Chapter 1
General Theory of Disperse Metal Electrodeposits Formation

Konstantin I. Popov and Nebojša D. Nikolić

1.1 Introduction

The most frequently used form of the cathodic polarization curve equation for flat or large spherical electrode of massive metal is given by

$$j = \frac{j_0(f_c - f_a)}{1 + \frac{j_0 f_c}{j_L}}, \tag{1.1}$$

where j, j_0 and j_L, are the current density, exchange current density, and limiting diffusion current density, respectively, and

$$f_c = 10^{\frac{\eta}{b_c}}, \tag{1.2}$$

K.I. Popov (✉)
ICTM-Institute of Electrochemistry, University of Belgrade, Njegoševa 12, P.O.B. 473,11001 Belgrade, Serbia

Faculty of Technology and Metallurgy, University of Belgrade, Karnegijeva 4, P.O.B. 3503,11001 Belgrade, Serbia
e-mail: kosta@tmf.bg.ac.rs

N.D. Nikolić
ICTM-Institute of Electrochemistry, University of Belgrade, Njegoševa 12, P.O.B. 473,11001 Belgrade, Serbia
e-mail: nnikolic@tmf.bg.ac.rs

Stojan S. Djokić (ed.), *Electrochemical Production of Metal Powders*, Modern Aspects of Electrochemistry 54, DOI 10.1007/978-1-4614-2380-5_1,

$$f_a = 10^{-\frac{\eta}{b_a}}, \tag{1.3}$$

where b_c and b_a are the cathodic and anodic Tafel slopes and η is the overpotential. Equation (1.1) is modified for use in electrodeposition of metals by taking cathodic current density and overpotential as positive. Derivation of Eq. (1.1) is performed under assumption that the concentration dependence of j_0 can be neglected [1–4].

It is known [3] that electrochemical processes on microelectrodes in bulk solution can be under activation control at overpotentials which correspond to the limiting diffusion current density plateau of the macroelectrode. The cathodic limiting diffusion current density for steady-state spherical diffusion, $j_{L,Sp}$ is given by

$$j_{L,Sp} = \frac{nFDC_0}{r}, \tag{1.4}$$

and for steady-state linear diffusion, j_L, it is given by

$$j_L = \frac{nFDC_0}{\delta}, \tag{1.5}$$

where n is the number of transferred electrons, F is the Faraday constant, D and C_0 are the diffusion coefficient and bulk concentration of the depositing ion, respectively, r is the radius of the spherical microelectrode, and δ is the diffusion layer thickness of the macroelectrode. It follows from Eqs. (1.4) and (1.5) that

$$\frac{j_{L,Sp}}{j_L} = \frac{\delta}{r}. \tag{1.6}$$

An electrode around which the hydrodynamic diffusion layer can be established, being considerably lower than dimensions of it, could be considered as a macroelectrode. An electrode, mainly spherical, whose diffusion layer is equal to the radius of it, satisfying

$$\delta \gg r, \tag{1.7}$$

can be considered as a microelectrode [5].

According to Eq. (1.1) for

$$f_c \gg f_a \text{ and } \frac{j_0 f_c}{j_L} \gg 1, \tag{1.8}$$

the cathodic process on the macroelectrode enters full diffusion control, i.e.,

$$j \cong j_L. \tag{1.9}$$

Simultaneously, the cathodic current density on the spherical microelectrode, j_{Sp}, is given by

$$j_{Sp} = \frac{j_0(f_c - f_a)}{1 + \frac{j_0 f_c}{j_{L,Sp}}} \tag{1.10}$$

or, because of Eq. (1.6),

$$j_{Sp} = \frac{j_0(f_c - f_a)}{1 + \frac{j_0}{j_L} \cdot \frac{r}{\delta} \cdot f_c} \tag{1.11}$$

and, if condition (1.8) is also valid, but

$$\frac{r}{\delta} \to 0. \tag{1.12}$$

Equation (1.11) can be rewritten in the form

$$j = j_0 f_c. \tag{1.13}$$

This means that the process on the microelectrode in the bulk solution can be under complete activation control at the same overpotential at which the same process on the macroelectrode is simultaneously under full diffusion control.[1]

[1] The reversible potential of a surface with radius of curvature r_{cur} would depart from that of a planar surface by the quantity $\Delta E_r = 2\sigma V/(nFr_{cur})$, where σ is the interfacial energy between metal and solution, and V is the molar volume of metal [5]. It is valid at extremely low r_{cur}, being of the order of few millivolts, and it can be neglected except in some special cases, like the stability of the shape of the tips of dendrites [5].

The different behavior of macroelectrodes and microelectrodes under the same conditions of electrodeposition causes the disperse deposits formation.

Since the paper of Barton and Bockris [5] on the growth of silver dendrites, a lot of papers, chapters, and even books, dealing with electrodeposition of disperse metals were published. The aim of this chapter is to unite the basic statements of the previous contributions in a general all-inclusive theory.

1.2 Active Microelectrodes Placed the Inside Diffusion Layer of the Active Macroelectrode

1.2.1 Basic Facts

Naturally, the microelectrodes can be placed on the macroelectrodes inside their diffusion layers. Let us consider the model of surface irregularities shown in Fig. 1.1. The electrode surface irregularities

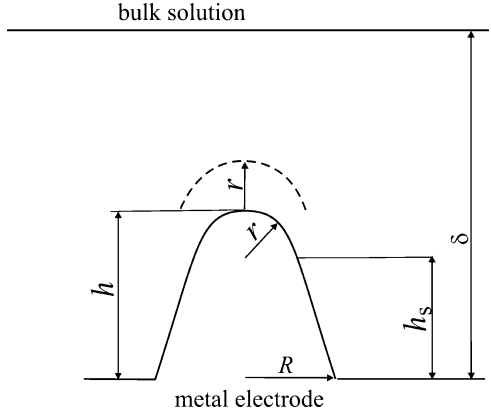

Fig. 1.1 Model of a paraboloidal surface protrusion: h is the height of the protrusion relative to the flat portion of the surface, h_s is the corresponding local side elongation, r is the radius of the protrusion tip, R is the radius of the protrusion base, δ is the thickness of the diffusion layer, and $\delta \gg h$ (Reprinted from [1] with permission from Springer and [6] with permission from Elsevier.)

are buried deep in the diffusion layer, which is characterized by a steady linear diffusion to the flat portion of the surface [1, 6, 7].

At the side of an irregularity, the limiting diffusion current density, $j_{L,S}$, is given as

$$j_{L,S} = \frac{nFDC_0}{\delta - h_s} = j_L \frac{\delta}{\delta - h_s}. \tag{1.14}$$

Obviously, this is valid if the protrusion height does not affect the outer limit of the diffusion layer and that a possible lateral diffusion flux supplying the reacting ions can be neglected. At the tip of an irregularity, the lateral flux cannot be neglected and the situation can be approximated by assuming a spherical diffusion current density, $j_{L,tip}$, given by [7]

$$j_{L,tip} = \frac{nFDC^*}{r}, \tag{1.15}$$

where C^* is the concentration of the diffusing species at a distance r from the tip, assuming that around the tip a spherical diffusion layer having a thickness equal to the radius of the protrusion tip is formed [5]. Obviously, if $R > \delta$ the spherical diffusion layer around the tips of protrusion cannot be formed and Eq. (1.16) is valid:

$$j_{L,tip} = \frac{nFDC_0}{\delta - h}. \tag{1.16}$$

If deposition to the macroelectrode is under full diffusion control, the distribution of the concentration C inside the linear diffusion layer is given by [3]

$$C = C_0 \frac{h}{\delta}, \tag{1.17}$$

where $0 \leq h \leq \delta$. Hence,

$$C^* = C_0 \frac{h + r}{\delta} \tag{1.18}$$

and

$$j_{\mathrm{L,tip}} = j_{\mathrm{L}}\left(1 + \frac{h}{r}\right) \tag{1.19}$$

because of Eqs. (1.5), (1.15), and (1.18).

The tip radius of the paraboloidal protrusion is given by [3, 5, 8]

$$r = \frac{R^2}{2h}, \tag{1.20}$$

and substitution of r from Eq. (1.20) in Eq. (1.19) gives

$$j_{\mathrm{L,tip}} = j_{\mathrm{L}}\left(1 + \frac{2h^2}{R}\right) \tag{1.21}$$

or

$$j_{\mathrm{L,tip}} = j_{\mathrm{L}}(1 + 2k^2), \tag{1.22}$$

where

$$k = \frac{h}{R}. \tag{1.23}$$

Hence for a hemispherical protrusion,
If $h = R$, $k = 1$

$$j_{\mathrm{L,tip}} = 3j_{\mathrm{L}}, \tag{1.24}$$

if $h << R$, $k \to 0$

$$j_{\mathrm{L,tip}} \to j_{\mathrm{L}}, \tag{1.25}$$

and if $R << h$, $k \to \infty$

$$j_{\mathrm{L,tip}} \to \infty. \tag{1.26}$$

Substituting $j_{L,tip}$ from Eq. (1.22) instead of j_L in Eq. (1.1) and further rearranging gives

$$j_{tip} = \frac{j_{0,tip}(f_c - f_a)}{1 + \frac{j_{0,tip}}{j_L} \cdot \frac{1}{1+2k^2} f_c}, \tag{1.27}$$

if j_0 around the tip is $j_{0,\,tip}$ and if the surface energy term [3, 5] can be neglected. The current density on the tip of a protrusion, j_{tip}, is determined by k, hence by the shape of the protrusion. If $k \to 0$, $j_{tip} \to j$ (see Eq. (1.1)) and if $k \to \infty$, $j_{tip} \to j_{0,\,tip}$ $(f_c - f_a) >> j$. The electrochemical process on the tip of a sharp needle-like protrusion can be under pure activation control outside the diffusion layer of the macroelectrode. Inside it, the process on the tip of a protrusion is under mixed control, regardless it is under complete diffusion control on the flat part of the electrode for $k \to 0$. If $k = 1$, hence for hemispherical protrusion, j_{tip} will be somewhat larger than j, but the kind of control will not be changed. It is important to note that the current density to the tip of hemispherical protrusion does not depend on the size of it if $k = 1$. This makes a substantial difference between spherical microelectrodes in bulk solution [9] and microelectrodes inside diffusion layer of the macroelectrode [3]. In the first case the limiting diffusion current density depends strongly on the radius of the microelectrode.

1.2.2 Physical Illustration

1.2.2.1 General Observation

Activation-controlled deposition of copper produces large grains with relatively well-defined crystal shapes. This can be explained by the fact that the values of the exchange current densities on different crystal planes are quite different, whereas the reversible potential is approximately the same for all planes [10, 11]. This can lead to preferential growth of some crystal planes, because the rate of deposition depends only on the orientation, which leads to the formation of a large-grained rough deposit. However, even at low

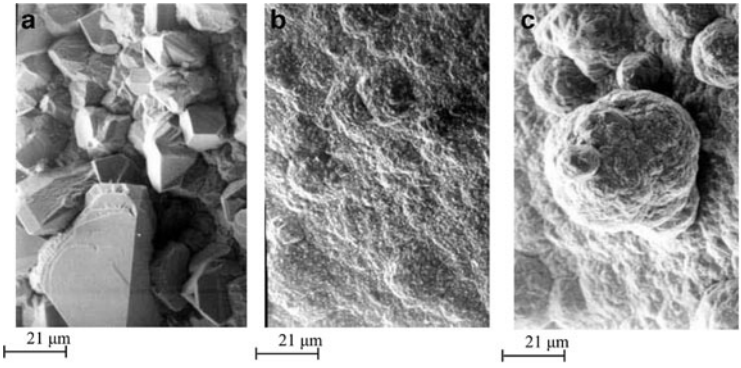

Fig. 1.2 Copper deposits obtained from 0.10 M $CuSO_4$ in 0.50 M H_2SO_4. Quantity of electricity, Q: 20 mAh cm^{-2}. (**a**) Activation-controlled deposition: deposition overpotential, η: 90 mV, initial current density: 3.3 mA cm^{-2}; (**b**) electrodeposition under mixed activation–diffusion control: $\eta = 140$ mV, initial current density: 4.2 mA cm^{-2}, and (**c**) electrodeposition under dominant diffusion control: $\eta = 210$ mV, initial current density 6.5 mA cm^{-2} (Reprinted from [7, 10] with permission from Springer and [12] with permission from Elsevier.)

degrees of diffusion control, the formation of large, well-defined grains is not to be expected, because of irregular growth caused by mass transport limitations. Hence, the current density which corresponds to the very beginning of mixed control (a little larger than this at the end of the Tafel linearity) will be the optimum one for compact metal deposition [12].

All the above facts are illustrated in Fig. 1.2 [12].

1.2.2.2 Cauliflower-Like Forms

It can be seen from Fig. 1.2c that the surface protrusions are globular and cauliflower-like. If the initial electrode surface protrusions are ellipsoidal shape, they can be characterized by the base radius R_0 and the height h as shown in Fig. 1.3a.

The tip radius is then given by

$$r = \frac{R_0^2}{h}. \tag{1.28}$$

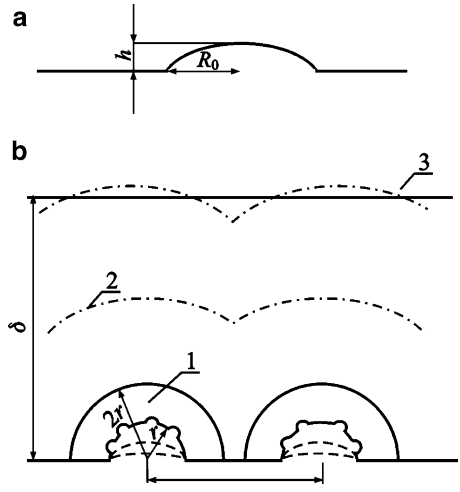

Fig. 1.3 Schematic representation of (**a**) the initial electrode surface protrusion and (**b**) the establishment of spherical diffusion layers around independently growing protrusions. (1) $r < (\delta - h)$ and $r < 1/4\ l$, spherical diffusion zones are formed; (2) $r < (\delta - h)$ and $r > 1/4\ l$, spherical diffusion zones overlap; (3) $r > (\delta - h)$, spherical diffusion zones are not formed (Reprinted from [13] with permission from the Serbian Chemical Society and [7, 10] with permission from Springer.)

The initial electrode surface protrusion is characterized by $h \to 0$ and $r \to \infty$ if $R_0 \neq 0$. In this situation, a spherical diffusion layer cannot be formed around the tip of the protrusion if $r < \delta - h$, and linear diffusion control occurs, leading to an increase in the height of the protrusion relative to the flat surface.

The rate of growth of the tip of a protrusion for $r > \delta$ is equal to the rate of motion of the tip relative to the rate of motion of the flat surface. Hence,

$$\frac{\mathrm{d}h}{\mathrm{d}t} = \frac{V}{nF}\left(j_{\mathrm{L,\,tip}} - j_{\mathrm{L}}\right). \tag{1.29}$$

Substituting $j_{\mathrm{L,tip}}$ from Eq. (1.16) and j_{L} from Eq. (1.5) in Eq. (1.29) and further rearranging gives

$$\frac{\mathrm{d}h}{\mathrm{d}t} = \frac{VDC_0}{\delta} h \tag{1.30}$$

or

$$h = h_0 \exp\left(\frac{VDC_0}{\delta^2} t\right). \tag{1.31}$$

When h increases, r decreases, and spherical diffusion control can be operative around the whole surface of protrusion, if it is sufficiently far from the other ones, as illustrated by Fig. 1.3b. In this situation, second-generation protrusions can grow inside the diffusion layer of first-generation protrusions in the same way as first-generation protrusions grow inside the diffusion layer of the macroelectrode and so on.

A cauliflower-like deposit is formed under such conditions, as is shown in Fig. 1.4. It can be seen from Fig. 1.4a that the distance between the cauliflower-like grains is sufficiently large to permit the formation of spherical diffusion zones around each of them. Simultaneously, second-generation protrusions grow in all directions, as shown in Fig. 1.4b, c. This confirms the assumption that the deposition takes place in a spherically symmetric fashion.

To a first approximation, the rate of propagation can be taken to be practically the same in all directions, meaning that the cauliflower-type deposit formed by spherically symmetric growth inside the diffusion layer of the macroelectrode will be hemispherical, as is illustrated in Fig. 1.4a–c.

This type of protrusion is much larger than that formed by linearly symmetric growth inside the diffusion layer of the macroelectrode (Fig. 1.4a–c).

This is because a spherical diffusion layer cannot be formed around closely packed protrusions, their diffusion fields overlap and they grow in the diffusion layer of the macroelectrode.

If spherical diffusion layer can be established around the tip of a protrusion the limiting diffusion current to the tip is given by Eq. (1.19) or by

$$j_{\mathrm{L,tip}} = j_{\mathrm{L}} \frac{h}{r} \tag{1.32}$$

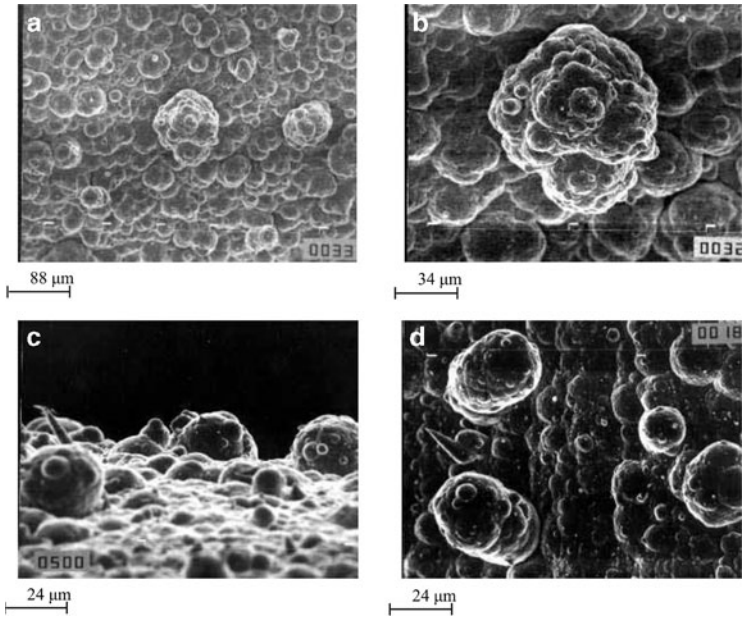

Fig. 1.4 Copper deposits obtained from 0.30 M $CuSO_4$ in 0.50 M H_2SO_4 by electrodeposition under mixed activation–diffusion control. Deposition overpotential: 220 mV (**a**) Quantity of electricity: 40 mAh cm^{-2}; (**b**) The same as in (**a**), and (**c**) and (**d**) quantity of electricity: 20 mAh cm^{-2} (Reprinted from [7, 10] with permission from Springer and [13] with permission from the Serbian Chemical Society.)

for

$$\frac{h}{r} \gg 1. \tag{1.33}$$

1.2.2.3 Carrot-Like Forms

It can also be seen from Figs. 1.4c, d and 1.5 that the growth of such protrusions produces carrot-like forms, another typical form obtained in copper deposition under mixed activation–diffusion control. This happens under the condition $k << 1$, when spherical diffusion

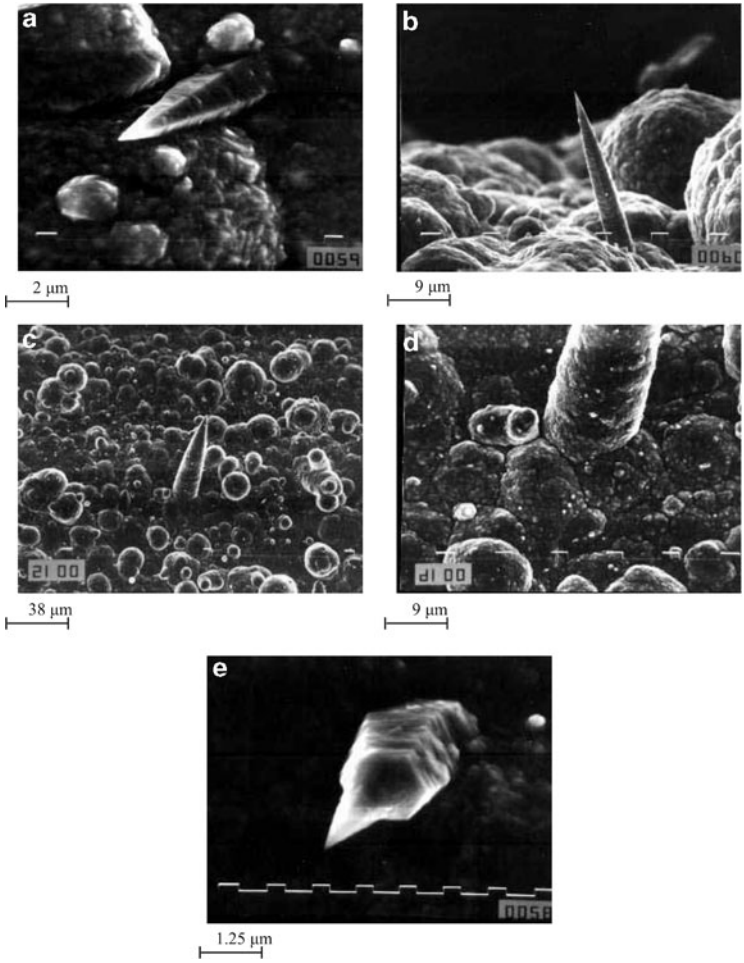

Fig. 1.5 Copper deposits obtained from 0.30 M $CuSO_4$ in 0.50 M H_2SO_4 by electrodeposition under mixed activation–diffusion control. Deposition overpotential: 220 mV. Quantity of electricity (**a**) 10 mAh cm^{-2}; (**b**) 40 mAh cm^{-2}; (**c**) 20 mAh cm^{-2}; (**d**) the root of the carrot from (**c**); and (**e**) 10 mAh cm^{-2} (Reprinted from [7, 10] with permission from Springer and [14] with permission from the Serbian Chemical Society.)

control takes place only around the tip of the protrusion, as is illustrated in Fig. 1.5. In this case, Eq. (1.27) can be rewritten in the form:

$$j_{\text{tip}} = j_{0,\text{tip}}(f_{\text{c}} - f_{\text{a}}), \tag{1.34}$$

meaning that deposition on the protrusion tip can be under pure activation control at overpotentials lower than the critical one for the initiation of dendritic growth.

This happens if the nuclei have a shape like that in Fig. 1.5. The assumption that the protrusion tip grows under activation control is confirmed by the regular crystallographic shape of the tip [14] just as in the case of grains growing on the macroclectrode under activation control (see Fig. 1.2a).

The maximum growth rate at a given overpotential corresponds to activation-controlled deposition. As a result, the propagation rate at the tip will be many times larger than that in other directions, resulting in protrusions like that in Fig. 1.5b. The final form of the carrot-like protrusion is shown in Fig. 1.5c. It can be concluded from the parabolic shape that such protrusions grow as moving paraboloids in accordance with the Barton–Bockris theory [5], the tip radius remaining constant because of the surface energy effect. It can be concluded from Fig. 1.5d that thickening of such a protrusion is under mixed activation–diffusion control because the deposit is seen to be of the same quality as that on the surrounding macroelectrode surface. It can be seen from Fig. 1.5e that activation control takes place only at the very tip of the protrusion.

1.2.3 The Essence of Dendritic Deposits Formation

Two phenomena seem to distinguish dendritic from carrot-like growth [15–17]:

1. A certain well-defined critical overpotential value appears to exist below which dendrites do not grow.
2. Dendrites exhibit a highly ordered structure and grow and branch in well-defined directions. According to Wranglen [18], a dendrite is a skeleton of a monocrystal and consists of a stalk and branches, thereby resembling a tree.

It is known that dendritic growth occurs selectively at three types of growth sites [16]:

1. Dendritic growth occurs at screw dislocations. Sword-like dendrites with pyramidal tips are formed by this process [3, 16].
2. Many investigations of the crystallographic properties of dendrites have reported the existence of twin structures [19–21]. In the twinning process, a so-called indestructible reentrant groove is formed. Repeated one-dimensional nucleation in the groove is sufficient to provide for growth extending in the direction defined by the bisector of the angle between the twin plants [16].
3. It is a particular feature of a hexagonal close-packed lattice that growth along a high-index axis does not lead to the formation of low index planes. Grooves containing planes are perpetuated and so is the chance for extended growth by the one-dimensional nucleation mechanism [22].

In all the above cases, the adatoms are incorporated into the lattice by repeated one-dimensional nucleation. On the other hand, deposition to the tip of screw dislocations can be theoretically considered as deposition to a point; in the other two cases, the deposition is to a line.

From the electrochemical point of view, a dendrite can be defined as an electrode surface protrusion that grows under activation or mixed control, while deposition to the flat part of the electrode surface is under complete diffusion control [3, 4, 8, 15].

Considering the model of surface irregularities shown in Fig. 1.1, the surface irregularities are buried deep in the diffusion layer, which is characterized by a steady linear diffusion to the flat portion of completely active surface.

If the protrusion does not affect the outer limit of the diffusion layer, i.e., if $\delta \gg h$, the limiting diffusion current density to the tip of the protrusion from Fig. 1.1, $j_{\mathrm{L,tip}}$, is given by

$$j_{\mathrm{L,tip}} = j_{\mathrm{L}}\left(1 + \frac{h}{r}\right). \tag{1.19}$$

Substitution of $j_{L,tip}$ from Eq. (1.19) into Eq. (1.1) produces for $h/r >> 1$:

$$j_{tip} = j_{0,tip}(f_c - f_a), \tag{1.34}$$

where $j_{0,tip}$ is the exchange current density at the tip of a protrusion.

Obviously, deposition to the tip of such protrusion inside the diffusion layer is activation-controlled relative to the surrounding electrolyte, but it is under mixed activation–diffusion control relative to the bulk solution.

If deposition to the flat part of electrode is a diffusion-controlled process and assuming a linear concentration distribution inside diffusion layer, the concentration C_{tip} at the tip of a protrusion can be given by modified Eq. (1.17) [3]

$$C_{tip} = C_0 \frac{h}{\delta}. \tag{1.17a}$$

According to Newman [23] the exchange current density at the tip of a protrusion is given by

$$j_{0,tip} = j_0 \left(\frac{C_{tip}}{C_0} \right)^{\xi}, \tag{1.35}$$

where

$$\xi = \frac{\mathrm{d} \log j_0}{\mathrm{d} \log C_0} \tag{1.36}$$

and j_0 is the exchange current density for a surface concentration C_0 equal to that in the bulk,

or

$$j_{0,tip} = j_0 \left(\frac{h}{\delta} \right)^{\xi} \tag{1.37}$$

because of Eq. (1.17a).

Taking into account Eq. (1.34), the current density to the tip of a protrusion is then given by

$$j_{\text{tip}} = j_0 \left(\frac{h}{\delta}\right)^{\xi} (f_{\text{c}} - f_{\text{a}}) \tag{1.38}$$

being under mixed control due to the $(h/\delta)^{\xi}$ term, which takes into account the concentration dependence of $j_{0,\text{tip}}$, expressing in this way a mixed-controlled electrodeposition process.

Outside the diffusion layer $h \geq \delta$, Eq. (1.38) becomes

$$j_{\text{tip}} = j_0 (f_{\text{c}} - f_{\text{a}}), \tag{1.39}$$

indicating pure activation control, as the $(h/\delta)^{\xi}$ term is absent.

For the dendrite growth, the current density to the tip of a protrusion formed on the flat part of the electrode surface growing inside the diffusion layer should be larger than the corresponding limiting diffusion current density [24]. Hence,

$$j_{\text{L}} < j_{\text{tip}}, \tag{1.40}$$

the protrusion grows as a dendrite.

In accordance with Eq. (1.40), instantaneous dendrite growth is possible at overpotentials larger than some critical value, η_{c}, which can be derived from Eq. (1.38) as shown in [15, 17]

$$\eta_{\text{c}} = \frac{b_{\text{c}}}{2.3} \ln \frac{j_{\text{L}}}{j_0} \left(\frac{\delta}{h}\right)^{\xi}, \tag{1.41}$$

and minimum overpotential at which dendritic growth is still possible, η_{i} is given by

$$\eta_{\text{i}} = \frac{b_{\text{c}}}{2.3} \ln \frac{j_{\text{L}}}{j_0} \tag{1.42}$$

for $f_{\text{c}} \gg f_{\text{a}}$, where h and δ are the protrusion height and the diffusion layer thickness, respectively. For very fast processes, when $j_0/j_{\text{L}} \gg 1$, and if $f_{\text{c}} \approx f_{\text{a}}$ but $f_{\text{c}} > f_{\text{a}}$, Eq. (1.41) becomes

$$\eta_{\text{c}} = \frac{\text{RT}}{nF} \frac{j_{\text{L}}}{j_0} \left(\frac{\delta}{h}\right)^{\xi} \tag{1.43}$$

and Eq. (1.42)

$$\eta_i = \frac{RT}{nF}\frac{j_L}{j_0}, \tag{1.44}$$

meaning that in the case of ohmic-controlled reactions, dendritic growth can be expected at very low overpotentials, or better to say, if $j_0 \to \infty$, instantaneous dendritic growth is possible at all overpotentials if only mass transfer limitations are taken into consideration.

In fact, dendrite propagation under such conditions is under diffusion and surface energy control, and η_c is then given by [5, 24]

$$\eta_c = \frac{8\sigma V}{nFh} \tag{1.45}$$

where σ is the interfacial energy between metal and solution and V is the molar volume of the metal, and minimum overpotential at which dendritic growth is still possible, η_i is given by

$$\eta_i = \frac{8\sigma V}{nF\delta}. \tag{1.46}$$

Hence, a critical overpotential for initiation dendritic growth is also expected in such cases, being of the order of few millivolts [15, 17, 24].

1.3 Polarization Curves

1.3.1 The Polarization Curve Equation for Partially Covered Inert Electrode

A mathematical model can be derived under the assumption that the electrochemical process on the microelectrodes inside the diffusion layer of a partially covered inert macroelectrode is under activation control, despite the overall rate being controlled by the diffusion layer of the macroelectrode [6, 25]. The process on the microelectrodes